International Journal of Engineering, Sciences and Technologies
ISSN : 3079-2045
https://www.ij-est.org/

Volume 2, issue 3, https://doi.org/10.70961/KNOX5703

# USING ARTIFICIAL INTELLIGENCE TO PREDICT THE LIMIT PRESSURES OF FOUNDATION SOILS

S. Mitsinjo Randrianarisoa[1], Dina Tsihafoy[2], Miora A. F. Rambinintsoa[3], Veroniaina Razafitrimo[4]

1- Dr. Ing., Institut Supérieur de Technologie d'Antananarivo, B.P 8122 Ampasapito, 101 Antananarivo, Madagascar
2- Civil Engineer, Ministère des Travaux Publics, Anosy, 101 Antananarivo, Madagascar
3- Civil Engineer, Ministère des Travaux Publics, Anosy, 101 Antananarivo, Madagascar
4- Professor, Institut Supérieur de Technologie d'Antananarivo, B.P 8122 Ampasapito, 101 Antananarivo, Madagascar

Corresponding author: S. Mitsinjo Randrianarisoa
Adress: Ecole du Génie Civil, Institut Supérieur de Technologie d'Antananarivo, B.P 8122 Ampasapito, 101 Antananarivo, Madagascar
e-mail : ramitsinjo@yahoo.fr
Phone number : +261 34 20 865 58

**Abstract**

In the infrastructure sector, soil investigation is essential for sizing the foundations of structures. The depth of investigation required by current regulations and depending on the scale of the project is becoming a major problem in Madagascar due to inadequate resources or limited capacity of testing equipment. As a result, engineers are forced to extrapolate unknown values beyond the pressuremeter diagram supplied by the laboratory. But a poor estimate could well lead to colossal errors, with harmful consequences for future structures. With this in mind, an innovative and formidable method such as artificial neural networks is being used to effectively predict the unknown limit pressures at which test equipment reaches its limit at depth. The foundation calculation based on Menard pressuremeter tests was our choice, and the approaches were carried out under the conditions of multilayer formal neurons with a non-looped structure. The simulation results confirm the effectiveness and robustness of the approaches, and the prediction of the pressuremeter diagram ideally reflects both logic and reality. Finally, to ensure the predictive power of the networks, a comparison of the calculation of the piles with the GEOFOND software was carried out with an error rate of 0.49%, followed by a performance analysis with a Nash-Sutcliffe coefficient of 0.9028, justifying the best fit of the model to the observed values. We have concluded that our neural models perform very well and can be used by our engineers with a high level of reliability.

**Keywords**

Peak load limit, deep foundations, GEOFOND, piles under mud, Menard pressure meter, neural networks

## 1- Introduction

In this age of globalisation, scientific and technological advances are so rapid that they can only be expressed as an exponential function. One advance that cannot be overlooked is that of information technology. It is in this field that we have seen the development of what is known as artificial intelligence, which is the design of systems capable of reproducing the behaviour of humans in their reasoning activities [1].

A sub-category of artificial intelligence is the neural network, which was born of an attempt to model the human brain mathematically, and is therefore capable of learning, predicting, classifying and deciding. Given these advantages, neural networks are widely used in machine learning, electronics and robotics. But this book also shows that the concept of the artificial neural network is also a very powerful tool in the field of foundation geotechnics.

In construction engineering, good infrastructure investigation is important, if not vital, for the long-term survival of future structures. However, the problem of deep soil investigation also arises in Madagascar due to inadequate resources or the limited capacity of testing equipment. In most cases, the piles are well over 20 meters deep, especially in the case of bridges and other large-scale structures. As a result, our engineers are obliged to extrapolate unknown values beyond the pressuremeter diagram supplied by the Laboratory. But we all know that a poor estimate could well lead to colossal errors, with harmful consequences for future structures.

The aim of this work is therefore to use neural networks to learn the evolution of the limiting pressure curve of the soil at depth and then predict the unknown values beyond the pressuremeter diagram.

International Journal of Engineering, Sciences and Technologies
ISSN : 3079-2045
https://www.ij-est.org/
Volume 2, issue 3, https://doi.org/10.70961/KNOX5703

## 2- Methods

### 2.1. Soils and foundations

#### 2.1.1. Soil investigation: Pressuremeter tests

Pressuremeter tests were carried out every meter of depth to obtain cross-sections of the ground and the intrinsic parameters of the soil, such as the pressuremeter modulus E and the limit pressure Pl. These are the basis for dimensioning the foundation. In fact, using the raw results of the pressiometric measurements leads to a stress/strain relationship in place. [2]
The test involves progressively applying pressure to the soil and assessing its resistance.
The apparatus used is the Menard pressure meter shown in Figure 1. It comprises:

- a Pressure-Volume Controller (PVC) comprising three (03) manometers and a tube containing water;
- a three-cell cylindrical probe with an external diameter of 60 mm and a capacity of 750 cm3. The central cell of the probe is inflated with water and the guard cells with gas.
- a tube connecting the probe and the control unit connected to a gas tank.

The current standard describing the principle and operation of these tests is NFP 94-110 [3].

In geotechnical engineering, the advantages and importance of pressuremeter tests are: knowledge of soil layers at depth, knowledge of intrinsic parameters for sizing a foundation, knowledge of soil characteristics for anchoring a foundation, etc.
Figure 2 shows the pressuremeter tests carried out in our study area in Antananarivo.

#### 2.1.2. Insulated pile under axial load

A pile is a slender foundation that transfers the loads of the structure onto layers of soil with sufficient mechanical characteristics to prevent the soil from breaking and to limit displacements to very low values [4].

The 3 main parts of a pile are the **head**, the **tip** and the **shaft** between the head and the tip, illustrated in Figure 3.

**Limit load** $Q_l$
A limit load $Q_l$ corresponds to ground failure. At the moment of failure, the load $Q_l$ is balanced by the following limit reactions of the soil:

- unit resistance of the soil under the tip $q_p$ leading to the tip limit load : $Q_p = q_p A_p$ where $A_p$ is the cross-sectional area of the point ;
- resistance $q_s$ due to soil friction on the lateral surface of the pile; if $q_s$ is the the unitary lateral friction limit, the lateral friction limit load is : $Q_s = q_s A_s$ where $A_s$ designates the lateral surface of the pile.

⇛ Thus, the limit load is given by : $Q_l = Q_p + Q_s$ (1)

**Creep load** $Q_c$

International Journal of Engineering, Sciences and Technologies
ISSN : 3079-2045
https://www.ij-est.org/
Volume 2, issue 3, https://doi.org/10.70961/KNOX5703

The curve representing the load applied to the pile as a function of the depth of driving shows an approximately linear part limited to a load $Q_c$ called the creep load. For loads greater than $Q_c$ , pile settlement no longer stabilises over time at constant load.
A creep load corresponds to the limit of the substantially linear part of the curve representing the load applied to the pile.

- Piles that do not sink into the ground: $Q_c = \frac{Q_p}{2} + \frac{Q_s}{1,5}$ (2)
- Piles pushing up the ground : $Q_c = \frac{Q_p}{1,5} + \frac{Q_s}{1,5} = \frac{Q_l}{1,5}$ (3)
- Piles pulling out of the ground : $Q_p = 0$ et $Q_c = \frac{Q_s}{1,5}$ (4)

Figure 4 illustrates the installation of the different types of pile.

### 2.1.3. Prediction of peak limit load Qp using the pressuremeter method

The peak limit load of an isolated pile is given by the form : $Q_p = A\, K_p\, P_{le}{}^*$ (5)

With $A$ : the cross-section of the tip ;

$K_p$ : the bearing capacity factor, which depends on the nature of the soil ;

And $P_{le}{}^* = \frac{1}{3\,a+b} \int_{D-b}^{D+3a} P_l{}^*(z)\, dz$ : the equivalent net limit pressure (6)

Figure 5 shows the equivalent limit pressure.

With : $b = \min(a\,;h)$ (7)

$a = \frac{B}{2}\ if\ B > 1m$ (8)

$a = 0{,}5\ m\ \ if\ B < 1m$ (9)

$h$ : Anchoring in the support soil layer

$P_l{}^*(z)$ is obtained by joining the various $P_l{}^*$measured by line segments on a linear scale.

## 2.2. Artificial Neural Network

An artificial neural network (ANN) is a mathematical model of the human brain, making it possible to construct a behavioral model from the data provided. A neural network consists of a weighted, oriented graph whose nodes symbolize neurons. These neurons have an activation function that enables them to influence other neurons in the network. Connections between neurons, known as synaptic links, propagate neuron activity with a weighting characteristic of the connection. The weighting of synaptic links is called synaptic weight.
Network topology refers to the way in which neurons are connected to each other across different layers. In general, we can distinguish two main classes of ANN according to their topologies: direct and looped networks.

### 4.2.1. Architecture

The multi-layer perceptron (MLP) is one of direct network, its most widely used neural networks for approximation, classification and prediction problems. It consists of an input layer, an output layer and one or more hidden layers. The elements of two adjacent layers are interconnected by weights that link the different layers, as shown in Figure 6. Its activation function is the ***hyperbolic tangent***. [5]

International Journal of Engineering, Sciences and Technologies
ISSN : 3079-2045
https://www.ij-est.org/
Volume 2, issue 3, https://doi.org/10.70961/KNOX5703

Let : $w_{nm}$ is the weights linking the input layer with the hidden layer;
$u_{mj}$ the weights linking the hidden layer with the output layer.

The components of the MLP input vector X will be weighted by the weights $w_{nm}$ and then passed to the hidden layer according to the following equations:

$$C_m = \sum_{n=1}^{N} x_n w_{nm} \qquad (10)$$

$$y_m = f(C_m) \qquad (11)$$

The outputs of the hidden layer will also be weighted by the $u_{mj}$ weights and then transmitted to the output layer according to the following equations:

$$O_j = \sum_{m=1}^{M} y_m u_{mj} \qquad (12)$$

$$t_j = g(O_j) \qquad (13)$$

$f$ and $g$ represent the activation functions of the neurons in the hidden layer and the output layer respectively. In our case, they are sigmoids.

The sigmoid function is : $f(x) = \frac{1}{1+e^{-\alpha x}}$ (14)

The derivative is : $f'(x) = \alpha . f(x)[1 - f(x)]$ (15)

In the case of our study, we have chosen an MLP network with one input layer, one output layer and a single hidden layer of neurons. Learning is supervised.

### 4.2.2. Learning algorithm

Learning consists of adapting the values of the weights in order to obtain the desired behaviour of the MLP. To do this, a database of examples is created, with each example consisting of an input vector and an appropriate output vector. A learning algorithm known as the gradient backpropagation algorithm was introduced in 1985 by Rumelhart et al [6].

The adaptation of the $u_{mj}$ weights linking the hidden layer to the output layer is as follows:

$$u_{mj}^{(i+1)} = u_{mj}^{(i)} + n_1 . (t_j - z_j) g'(O_j) y_m \qquad (16)$$

The $w_{nm}$ weights linking the input layer to the hidden layer are updated as follows :

$$w_{nm}^{(i+1)} = w_{nm}^{(i)} + n_2 . \left\{ \sum_{j=1,i=1}^{J} (t_j - z_j) g'(O_j) u_{mj} \right\} (f'(c_m))(x_n) \qquad (17)$$

$n_1$ and $n_2$ are the learning steps.

## 2.3. Prediction of limit pressures using neural networks

In this study, it is the output itself that will be determined using the neural network. To do this, follow the steps below:

- the first step is to train the network: the network must be taught the evolution of the limiting pressures over the 70% of the database supplied by the Laboratory;

- the next step is to predict the limit pressure in the layer just beyond the known depths. The limit pressure found will in turn be considered as a known input that will be taught to the network, which will then predict the next result. These procedures are repeated until the desired maximum depth is reached.

- the final stage involves testing. To assess the performance of the prediction, it is therefore necessary to compare the remaining 30% of the database with real, complete results.

The neural network prediction algorithm is summarised in Figure 7.

NB: it should be pointed out here that there is no mathematical relationship between the input variables (depth Z [metre]) and the outputs (limiting pressures Pl [MPa]). The network learns the evolution and logic of the curve according to the nature of the soil at depth, and uses its predictive capacity for unknown values.

## 3- Results

### 3.1. Résultats des essais pressiométriques

According to the hand auger survey carried out on site, we have :

Below Pr2, the site consists of :
- at 1.80m: slightly yellowish micaceous sandy clayey silt;
- 1.80 to 4.60m: grey micaceous clay;
- 4.60 to 8.40m: blackish clayey peat;
- 8.40 to 11.00m: fine to micaceous grey sand;
- below this, a layer of compact grey clayey sand.

Below Pr1, the site consists of:
- 0.00 to 2.50m: slightly yellowish micaceous sandy clayey silt;
- 2.50 to 4.50m: slightly sandy, greyish micaceous clay;
- 4.50 to 7.60m: blackish clayey peat;
- 7.60 to 8.40m: greyish sandy clay;
- 8.40 to 10.60m: fine to medium grey sand;
- 10.60 to 12.00m: compact grey clayey sand;
- below this, a layer of medium grey sand.

The results of the pressuremeter tests are summarised in Table 1.

From these results, we can plot the pressuremeter diagrams for Pr2 and Pr1 in Figure 8 and Figure 9.

### 3.2. Results of calculation of the peak limit load

In this paragraph, we consider the results of the pressuremeter tests on the Pr2 borehole. The assumptions for calculating the pile's peak limit load are as follows:
- pile diameter: **d = 0.50 m** ;
- pile installation: **concrete pile under mud**;
- total height: **H = 20.00 m**;
- anchorage in the bearing soil layer: **D = 0.75 m**.

The GEOFOND software gives us the result shown in Figure 10.

Using this software, the peak limit load of the following pile Pr2 is: ***Qpu = 0.102 MN***

Excel programming was then carried out in order to compare the calculation results with the GEOFOND software. This programming would be very useful for calculating the peak limit load of the pile after prediction by the neural network.
The calculation is run and the results are shown in Figure 11.

After calculation in Excel, we found a peak limit load ***Qpu = 0.1021 MN*** which is almost equal to the value found with the GEOFOND software (Qpu = 0.102 MN). This confirms the reliability of our programming, with an error of 0.097%, which could be used for other necessary calculations.

### 3.3. Results of limit pressure prediction using neural networks

Let's continue with the results of the pressuremeter tests following the Pr2 borehole. This diagram is extended to a depth of 27 meters, but will be divided in two for the remainder of our simulation, including :

- at 0.00 to 20.00 meters: learning the neural network;
- at 20.00 to 27.00 meters: prediction and testing of the neural network.

#### 5.3.1. Training

With a number of neurons equal to 37, the pressuremeter diagram Pr2 from 0.00 to 20.00 metres is easily approximated by the single hidden layer perceptron network. The learning performance is $9.2379*10^{-10}$ and the equation of the regression line is of the form $Output = 1*Target + 3.4*10^{-6}$. The learning is supervised. Figure 12 shows the results of training the network.

At first sight, the two curves (real and approximate) are completely consistent with an architecture MLP [1-37-1-1]. In fact, the neural network was able to approximate the pressuremeter diagram with an error deviation of around $10*10^{-5}$ MPa, which is tolerable. Figure 13 shows the training error of the network.

During training, the value of RMSE = $3.0394*10^{-5}$ is very satisfactory. The network is thus capable of learning the evolution of the boundary pressure of the ground to a depth of 20.00 meters, and we can now move on to prediction.

#### 5.3.2. Prediction

The idea here is to transform each predicted value into an input. In effect, the network learns the new data in order to predict the next value up to p = 27.00 meters.
In our case, the prediction values can be perceived every meter ($\delta$ = 1.00 meter). Figure 14 illustrates this.

The result fits well because we have an increasing curve that verifies the growth of the compactness of the sand layer with depth. The result obtained is therefore logical and usable. Nevertheless, the degree of reliability of the result remains to be determined.

#### 5.3.3. Network test

Normally, the test should be carried out with the data that could not be used in the training. In other words, the values of the limiting pressures predicted by the network in the interval from 20.00 to 27.00 meters will be compared with the whole of the real pressuremeter diagram. Figure 15 shows the result of the prediction test.

This test allows us to see that the shape of the curve predicted by the network agrees well with the shape of the actual curve. We can therefore say that the prediction of the limiting pressures by the neural network is feasible, but with an error. Figure 16 shows a zoom of the prediction test (Figure 16a) and the prediction error deviation (Figure 16b).

There is an error difference between these two curves, the indicators of which are MAE = 0.062, MSE = 0.0083 and RMSE = 0.0909, which are very satisfactory. The method can therefore be applied to the other Pr1 diagram.

### 5.3.4. Validation

To validate the reliability of our results, let's take the values of the limit pressures from 0.00 to 20.00 meters and then compare the results of the calculation of the peak limit load by the GEOFOND software on the one hand and according to the values predicted by the network up to 27 meters on the other.

- With GEOFOND software, when the data was stopped at a depth of 20.00 meters, the software automatically extrapolated the data to calculate the limits of integration of the peak limit load. The results are shown in Figure 17.

After extrapolation by the software, the peak limit load of the following pile Pr2 is: ***Qpu = 0.101 MN***

- Using our Excel program, Figure 18 gives us the result of calculating the peak limit load according to the values predicted by the neural network up to 27.00 meters.

When we stopped at a depth of 20.00 meters, the calculations based on the values predicted by the neural network up to 27.00 meters gave us a peak limit load ***Qpu = 0.1015 MN*** which is almost equal to the value found with the GEOFOND software (Qpu = 0.101 MN) with an error of 0.49% which is very satisfactory.

Following our Excel programming, Table 2. gives us the values of each actual and predicted peak limit load by varying the total plug of the pile in the ground:

The error deviation indicators are MAE = 0.00978, MSE = 0.00014 and an error standard deviation $\sigma_{error}$ = 0.00720, which are all very satisfactory. This allows us to validate our network with permissible errors.

The Nash-Sutcliffe criterion is one of the performance indicators [7]. It estimates the ability of a model to reproduce observed behaviour and is calculated as follows:

$$NS = 1 - \frac{MSE}{\sigma_Y^2} \rightarrow NS = 1 - \frac{\sum_{i=1}^{n}\left(Y_{réel,i} - Y_{préd,i}\right)^2}{\sum_{i=1}^{n}\left(Y_{réel,i} - \overline{Y_{réel}}\right)^2} \quad (18)$$

In our case, NS = 0.9028 on the values of the peak limit load of the piles, which could be interpreted as follows:
- it is fairly close to 1, which means that the model fits the observed values better;
- it is greater than 0.7, indicating that the model is satisfactory, i.e. that the model and the observed values are consistent.

## 4- Discussions

International Journal of Engineering, Sciences and Technologies
ISSN : 3079-2045
https://www.ij-est.org/
Volume 2, issue 3, https://doi.org/10.70961/KNOX5703

Our study was based on a single pressuremeter test result (named Pr2), but in order to clarify the reliability of limit pressure prediction by artificial neural network, the simulation results based on the various pressuremeter tests supplied by the Laboratory are given below :

### 4.1. Pressuremeter test Pr1

With a number of 32 neurons, the Pr1 pressuremeter diagram is easily approximated by the single-layer hidden perceptron network between 0.00 and 11.00 meters with an average error of $1.76*10^{-6}$. Learning was stopped at a depth of 11.00 meters in the compact grey clayey sand layer. Figure 19 shows the results.

Here, the shape of the predicted curve agrees well with the actual curve. In other words, the neural network detected a peak from 11.00 meters and the curve generated decreases to a depth of 14.00 meters, justifying the logic whose prediction error deviation indicators between 11.00 and 14.00 meters are MAE = 0.1592, MSE = 0.0411 and a standard error deviation of 0.1449.

### 4.2. Pressuremeter test at KP 6+800 between Iavoloha - Ivato

With a number of 76 neurons, the pressuremeter diagram is easily approximated by the single-layer hidden perceptron network between 0.00 and 11.00 meters with an average error of $1.91*10^{-7}$. Learning was stopped at a depth of 11.00 meters in the compact purplish sandy clay layer. Figure 20 shows the results.

The result predicted by the network agrees well because we have an increasing curve which verifies the growth of the compactness between the layer of sandy clay towards the layer of clayey sand located at a depth of 12.00 meters. The result obtained is therefore logical, with the prediction error deviation indicators between 11.00 and 15.00 meters being MAE = 0.1071, MSE = 0.020 and a standard error deviation of 0.1035.

### 4.3. Pressuremeter test on a bridge at Soamanandrariny

With a number of 59 neurons, the pressuremeter diagram is easily approximated by the perceptron network with a single hidden layer between 0.00 and 16.00 meters with an average error of 6.978*10-5. Learning was stopped at a depth of 16.00 meters in the pinkish clayey silt layer. Figure 21 shows the results.

Between 16.00 and 18.00 meters, the network initially has a little difficulty adapting to the progression of the pressuremeter diagram, but from a depth of 18.00 meters the curve becomes increasing, verifying the growth in compactness towards the yellow silty clay layer. The result obtained reflects the logic and whose prediction error deviation indicators between 16.00 and 23.00 meters are MAE = 0.3370, MSE = 0.1754 and a standard error deviation of 0.2658.

## 5- Conclusion

In this study, the MLP neural model was trained by determining the weights and biases, using the Gradient Error Backpropagation algorithm. The use of the neural network is advantageous from a computational point of view, due to its speed. It generates prediction errors, but it is also reliable, as demonstrated by the results found in this research. In addition, the neural network adapts to the evolution of new computer technologies. In practice, it provides a solution to the problems faced by engineers in estimating the limiting pressures of deep-seated soils for the proper design of foundation structures.

This work is limited just to the use of MLP neural networks with a type of supervised learning. Amelioration can be made using other types of networks such as RBF or using semi-supervised learning.

## 6- References

[1] Esma Aïmeur « *Intelligence artificielle : quel avenir ?* », Université de Montréal, Département d'informatique et recherche opérationnelle (2004)

[2] COSTET G. SANGLERAT (1983) – *cours pratique de mécanique des sols* (Tome 2), 237 pages

[3] ARVOR Géotechnique, Fiche MPE-FT-08 A 2010 : *Essai pressiométrique Ménard sans cycle (NF P 94-110-1)*

[4] Ministère de l'équipement, du logement et des transports (1993)- *Règles techniques de conception et de calcul des fondations des ouvrages du Génie Civil – Fascicule 62 titre V*

[5] H. EL Badaoui , A. Abdallaoui et S. Chabaa (2014). *Perceptron Multicouches et réseau à Fonction de Base Radiale pour la prédiction du taux d'humidité*. International Journal of Innovation and Scientific Research ISSN 2351-8014 Vol. 5 No. 1 Jul. 2014, pp. 55-67

[6] D. Rumelhart, G. Hinton & R. Williams, "*Learning internal representations by error propagation," Parallel Distributed Processing*, Vol. 1., D. Rumelhart and J. McClelland Eds. Cambridge: MIT Press, pp. 318-362, 1986.

[7] [4.24] GRAIE, *Critères et indicateurs d'auto-évaluation des modèles*, Version 1 – Document de travail Mars 2018

International Journal of Engineering, Sciences and Technologies
ISSN : 3079-2045
https://www.ij-est.org/
Volume 2, issue 3, https://doi.org/10.70961/KNOX5703

## 7- Tables

**Table 1. Results of pressuremeter tests**

| Soil investigation | Depth (m) | 1 | 2 | 3 | 4 | 5 | 6 | 7 | 8 | 9 | 10 | 11 | 12 | 13 | 14 |
|---|---|---|---|---|---|---|---|---|---|---|---|---|---|---|---|
| Pr1 | Pl (MPa) | 0.15 | 0.08 | 0.12 | 0.10 | 0.16 | 0.19 | 0.23 | 0.54 | 0.65 | 0.76 | 1.37 | 0.82 | 0.79 | 0.65 |
| | E (MPa) | 1.97 | 1.03 | 1.03 | 1.02 | 1.04 | 1.46 | 1.49 | 4.48 | 5.59 | 7.02 | 12.0 | 7.80 | 7.15 | 6.93 |
| Pr2 | Pl (MPa) | 0.19 | 0.06 | 0.08 | 0.12 | 0.11 | 0.20 | 0.23 | 0.24 | 0.70 | 1.36 | 0.84 | 0.71 | 0.69 | |
| | E (MPa) | 5.58 | 0.87 | 0.76 | 1.36 | 1.12 | 1.48 | 1.41 | 1.41 | 6.76 | 12.7 | 7.43 | 7.30 | 7.01 | |

**Table 2. Error deviations of limit loads according to pile sheet**

| **total pile height (m)** | **20.00** | **21.00** | **22.00** | **23.00** | **24.00** | **25.00** |
|---|---|---|---|---|---|---|
| Actual limit load | 0.1021 | 0.1106 | 0.1387 | 0.1741 | 0.1937 | 0.1963 |
| Predicted limit load | 0.1015 | 0.1062 | 0.1504 | 0.1957 | 0.2049 | 0.2055 |
| Error deviation (MN) | **0.0006** | **0.0044** | **0.0117** | **0.0216** | **0.0112** | **0.0092** |

International Journal of Engineering, Sciences and Technologies
ISSN : 3079-2045
https://www.ij-est.org/

Volume 2, issue 3, https://doi.org/10.70961/KNOX5703

## 8- Figures

**Figure 1. Pressuremeter**

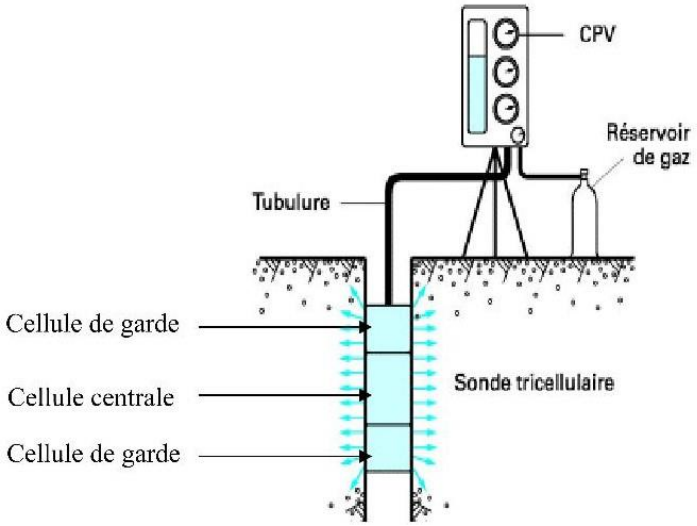


**Figure 2. Soil reconnaissance tests using a Menard pressuremeter**

***Source* : authors**

International Journal of Engineering, Sciences and Technologies
ISSN : 3079-2045
https://www.ij-est.org/

Volume 2, issue 3, https://doi.org/10.70961/KNOX5703

**Figure 3. Axial load curve of a pile**

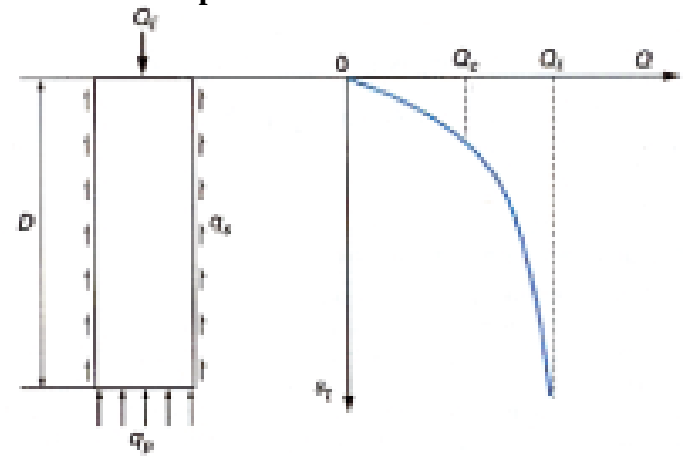


$D$ profondeur du pieu
$Q$ charges en tête
$Q_c$ charge de fluage
$Q_l$ charge limite
$q_p$ résistance unitaire de pointe
$q_s$ frottement latéral unitaire limite
$s_T$ enfoncement en tête

**Figure 4. Installation of different types of piles**

*a) pile drilling*

*b) reinforcement of piles*

International Journal of Engineering, Sciences and Technologies
ISSN : 3079-2045
https://www.ij-est.org/
Volume 2, issue 3, https://doi.org/10.70961/KNOX5703

*c) cased drilled pile* *d) concreted pile under mud*

*Source : authors*

**Figure 5. Equivalent pressure limit**

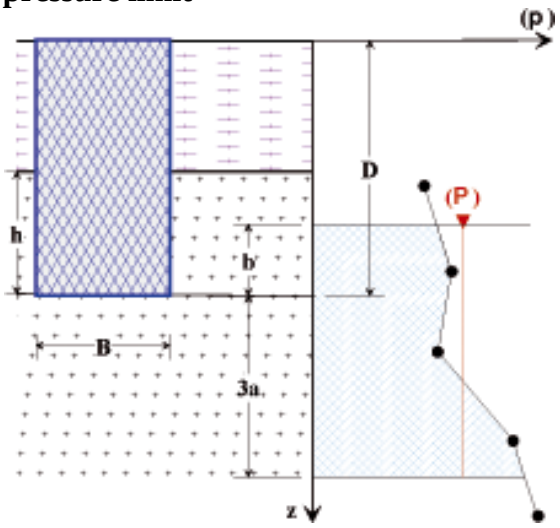


**Figure 6. MLP network architecture**

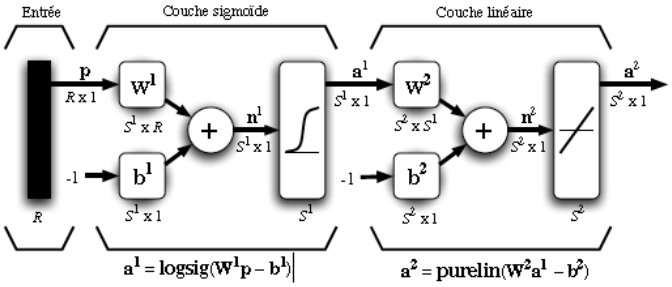


**Figure 7. Neural network prediction algorithm**

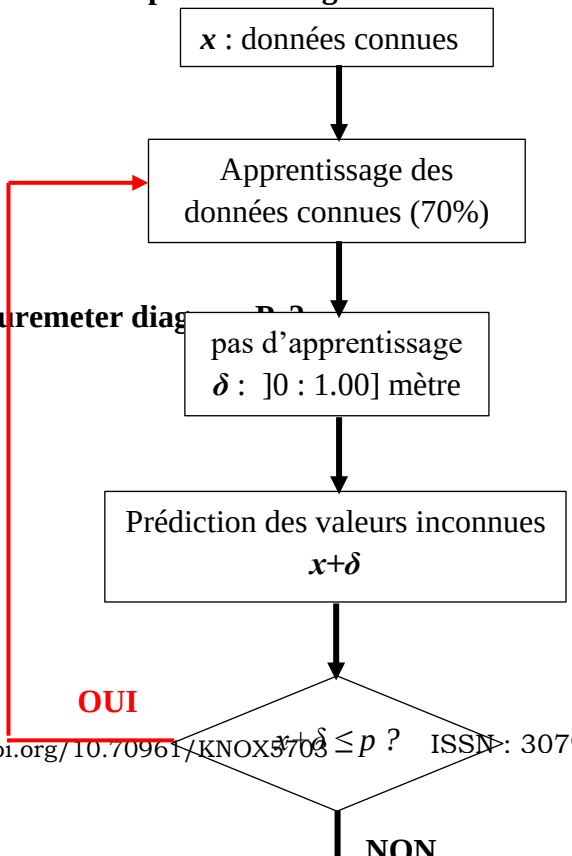


**Figure 8. Pressuremeter diag**

International Journal of Engineering, Sciences and Technologies
ISSN : 3079-2045
https://www.ij-est.org/
Volume 2, issue 3, https://doi.org/10.70961/KNOX5703

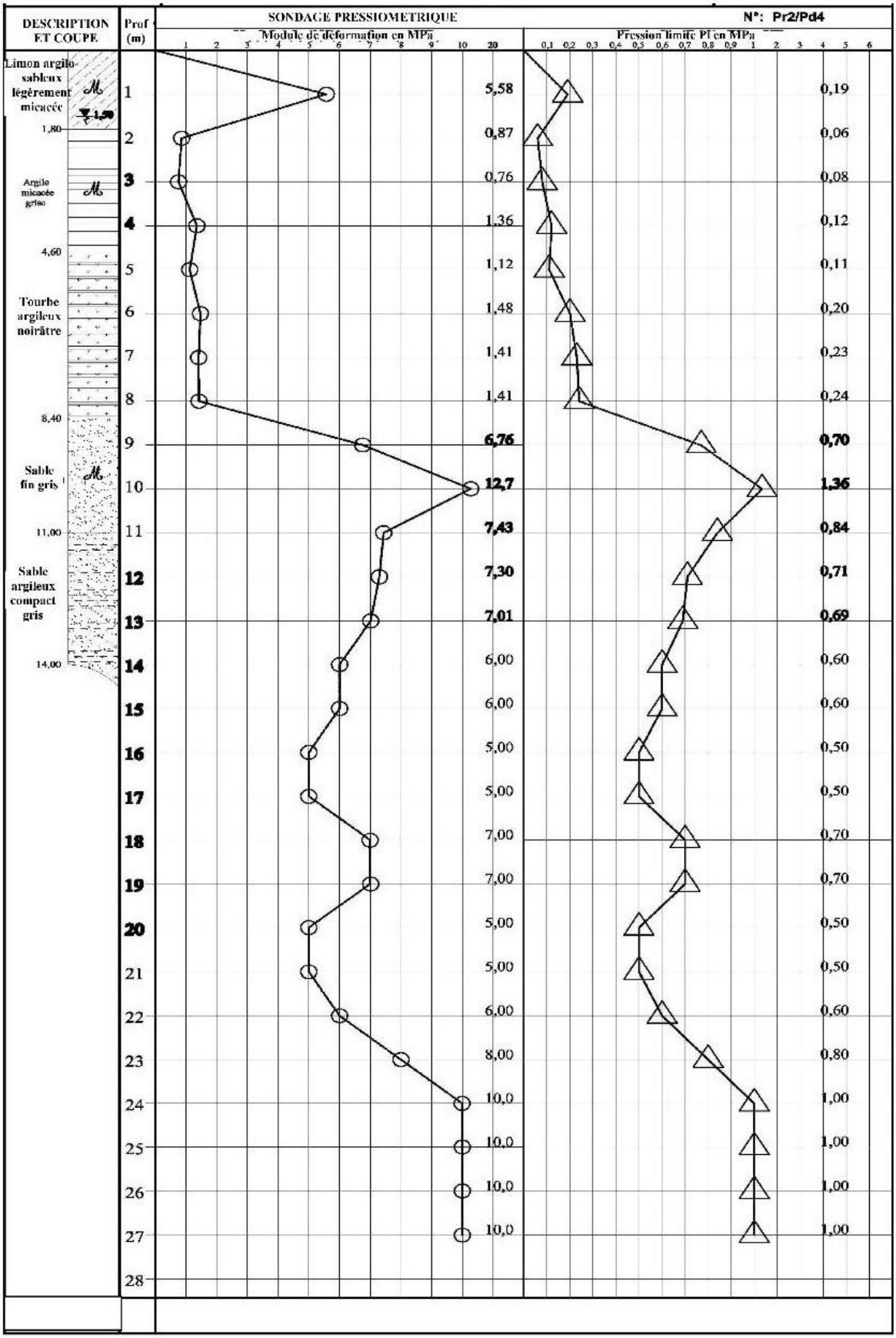

International Journal of Engineering, Sciences and Technologies
ISSN : 3079-2045
https://www.ij-est.org/
Volume 2, issue 3, https://doi.org/10.70961/KNOX5703

**Figure 9. Pressuremeter diagram Pr1**

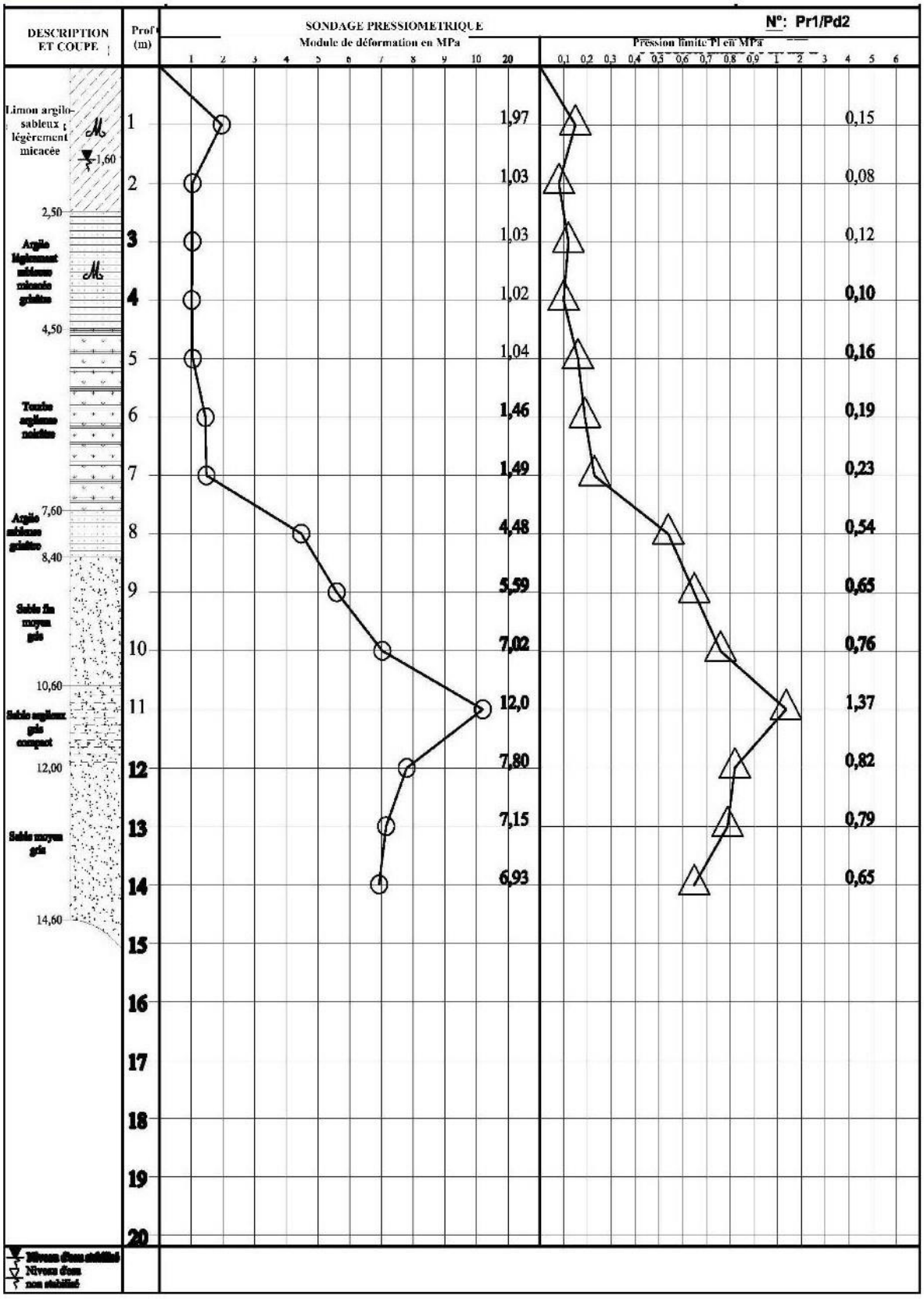

International Journal of Engineering, Sciences and Technologies
ISSN : 3079-2045
https://www.ij-est.org/
Volume 2, issue 3, https://doi.org/10.70961/KNOX5703

**Figure 10. Pile calculation using GEOFOND software based on actual data**

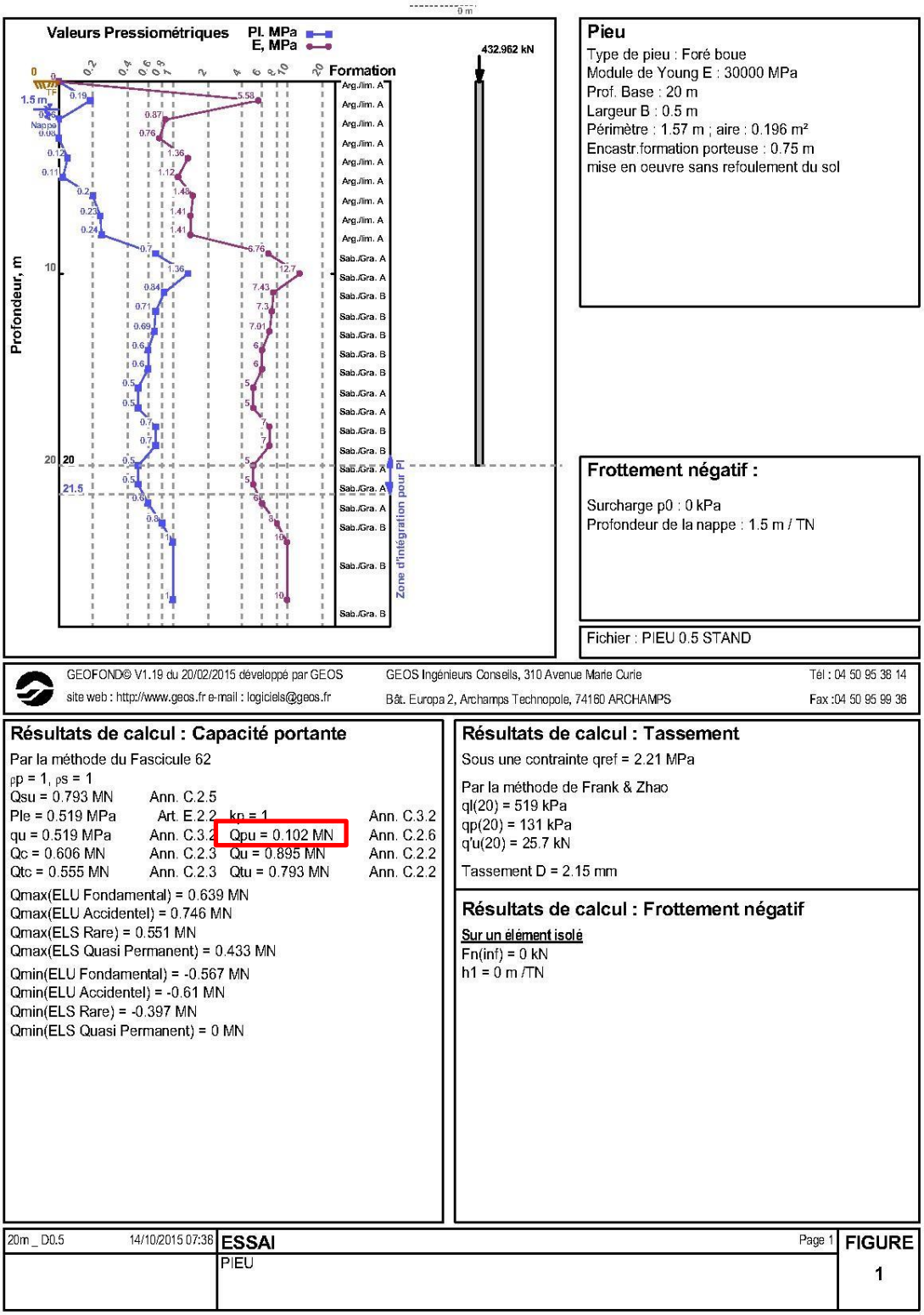

International Journal of Engineering, Sciences and Technologies
ISSN : 3079-2045
https://www.ij-est.org/
Volume 2, issue 3, https://doi.org/10.70961/KNOX5703

**Figure 11. Evaluation of the peak load limit using Excel based on actual data**

**PIEU FLOTTANT SOUS CHARGE AXIALE (fondation profonde : D/B > 10)**

Fascicule 62 titre V — Résultat expérimental (réel)

**1 RESULTATS ESSAI PRESSIOMETRIQUE (Préssiomètre Ménard)**

| Z (m) | E [Mpa] | Pl [Mpa] |
|---|---|---|
| 1 | | 0,19 |
| 2 | | 0,06 |
| 3 | | 0,08 |
| 4 | | 0,12 |
| 5 | | 0,11 |
| 6 | | 0,20 |
| 7 | | 0,23 |
| 8 | | 0,24 |
| 9 | | 0,70 |
| 10 | | 1,36 |
| 11 | | 0,84 |
| 12 | | 0,71 |
| 13 | | 0,69 |
| 14 | | 0,60 |
| 15 | | 0,60 |
| 16 | | 0,50 |
| 17 | | 0,50 |
| 18 | | 0,70 |
| 19 | | 0,70 |
| 20 | | 0,50 |
| 21 | | 0,50 |
| 22 | | 0,60 |
| 23 | | 0,80 |
| 24 | | 1,00 |
| 25 | | 1,00 |
| 26 | | 1,00 |
| 27 | | 1,00 |

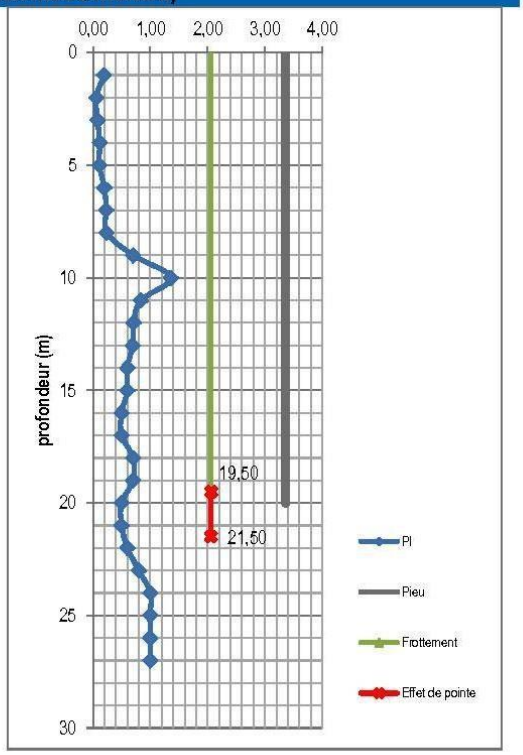


**2 CARACTERISTIQUES DU PIEU**

| | | | | |
|---|---|---|---|---|
| Géométrie du pieu | Circulaire | B = | 0,50 | m |
| | | P = | 1,57 | m |
| | | S = | 0,20 | m² |
| Longueur du pieu dans le sol | | D = | 20 | m |
| Type de mise en œuvre du pieu | | Pieu bétonné sous boue | | |
| Caractéristique du pieu | | Pieu béton | | |
| Si différent de pieu béton (*) | | Sables | | |

| | | | |
|---|---|---|---|
| Mise en œuvre du pieu | Mis en oeuvre sans refoulement du sol | | |
| ancrage du pieu dans la couche porteuse | h = | 0,75 | m |

**3 CARACTERISTIQUES DU SOL**

| | | | |
|---|---|---|---|
| Type du sol d'assise | Sables - Graves - A | | |
| Facteur de portance du sol | Kp = | 1,00 | |

**4 CHARGE LIMITE DE POINTE : Qp**

| | | | |
|---|---|---|---|
| Paramètres | a = | 0,50 | m |
| | b = | 0,50 | m |
| Bornes d'intégration de la pression limite équivalente | D - b = | 19,50 | m |
| | D + 3a = | 21,50 | m |
| Pression limite nette équivalente | Ple* = | 0,520 | Mpa |
| contrainte de rupture sous la pointe | qu = | 0,520 | Mpa |
| **Charge limite de pointe** | **$Q_{pu}$ =** | **0,1021** | **MN** |

**Figure 12. Neural network training results**

International Journal of Engineering, Sciences and Technologies
ISSN : 3079-2045
https://www.ij-est.org/

Volume 2, issue 3, https://doi.org/10.70961/KNOX5703

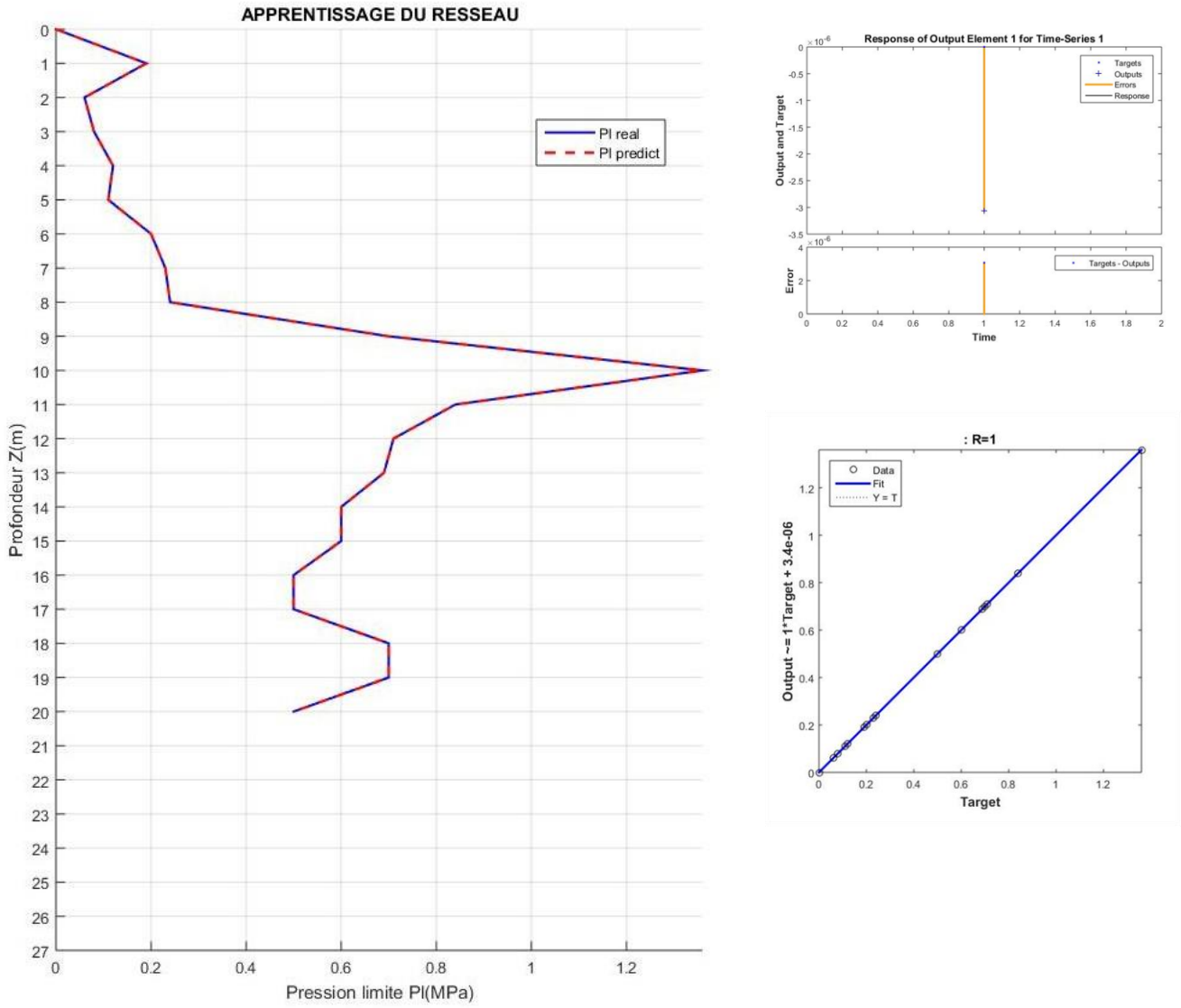


**Figure 13. Network learning error deviation**

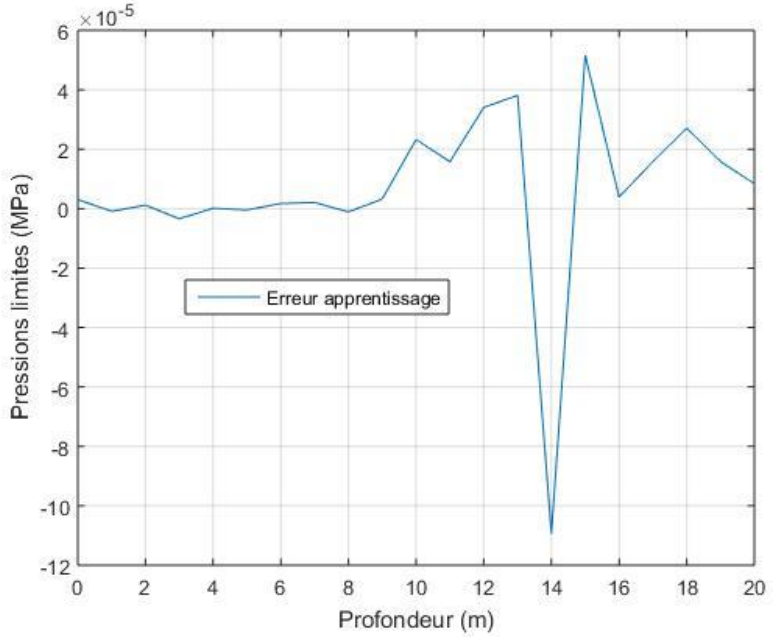

International Journal of Engineering, Sciences and Technologies
ISSN : 3079-2045
https://www.ij-est.org/
Volume 2, issue 3, https://doi.org/10.70961/KNOX5703

**Figure 14. Pressuremeter diagram predicted by the network**

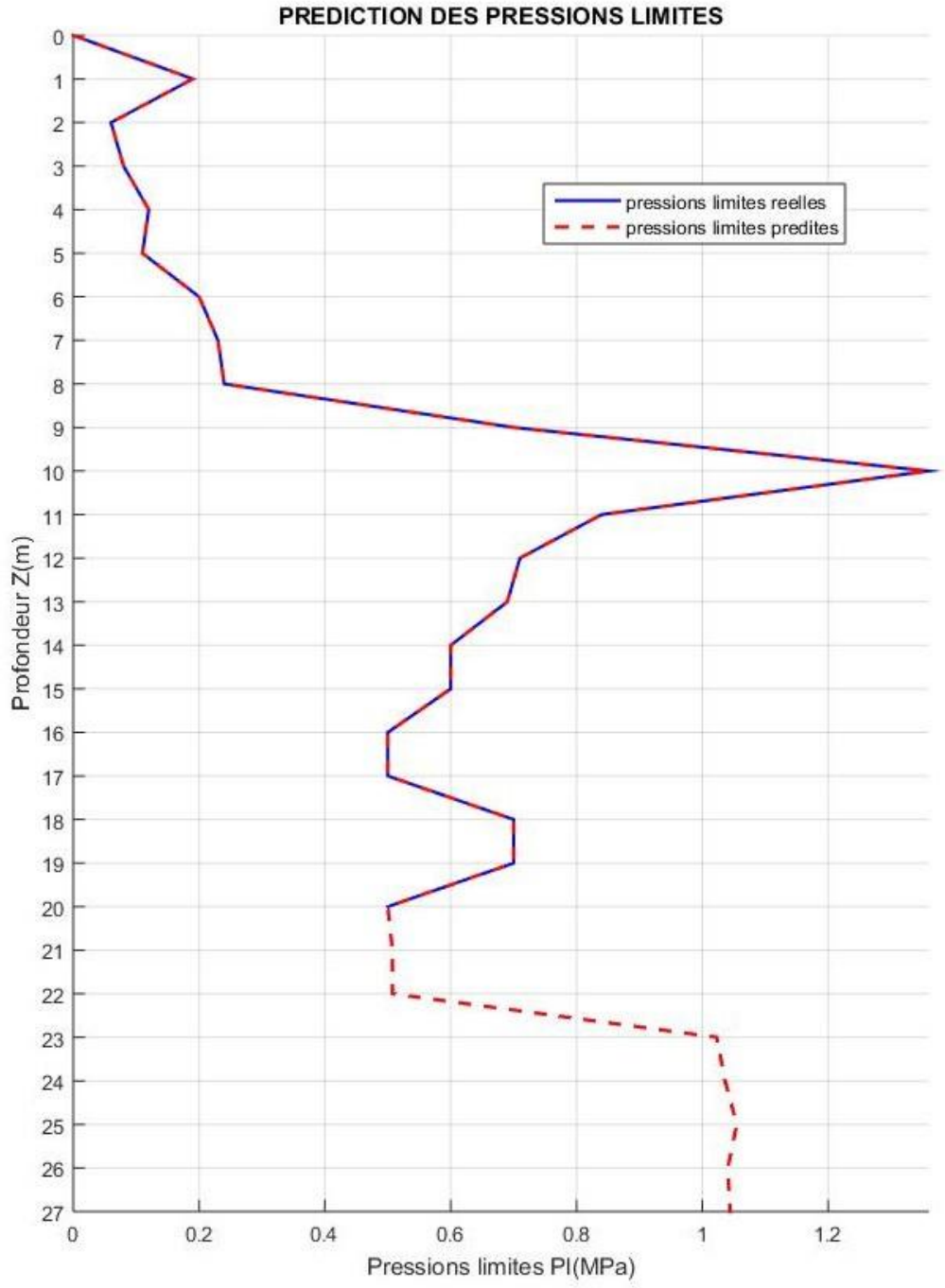

International Journal of Engineering, Sciences and Technologies
ISSN : 3079-2045
https://www.ij-est.org/
Volume 2, issue 3, https://doi.org/10.70961/KNOX5703

**Figure 15. Pressuremeter diagram prediction test**

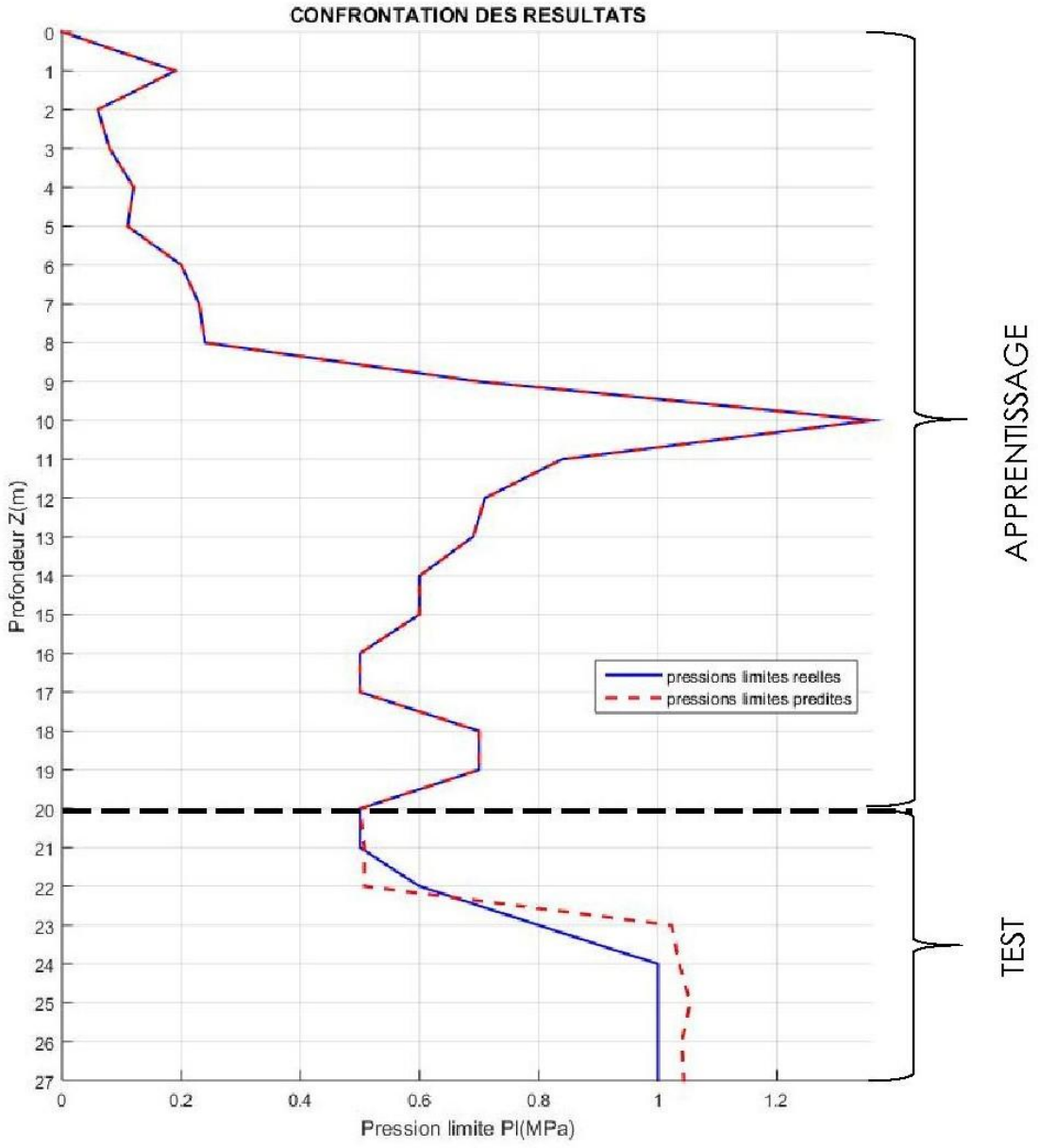


**Figure 16. Prediction test and error difference between 20 and 27 metres**

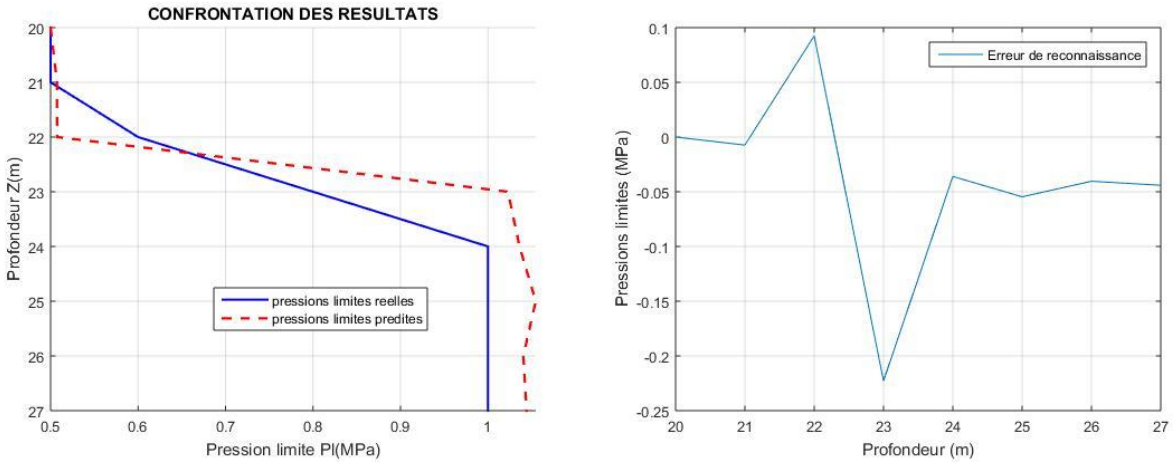

International Journal of Engineering, Sciences and Technologies
ISSN : 3079-2045
https://www.ij-est.org/

Volume 2, issue 3, https://doi.org/10.70961/KNOX5703

*a) prediction test at 20-27m* *b) prediction error range 20-27m*

**Figure 17. Calculation of the pile using GEOFOND software at 0.00-20.00 m**

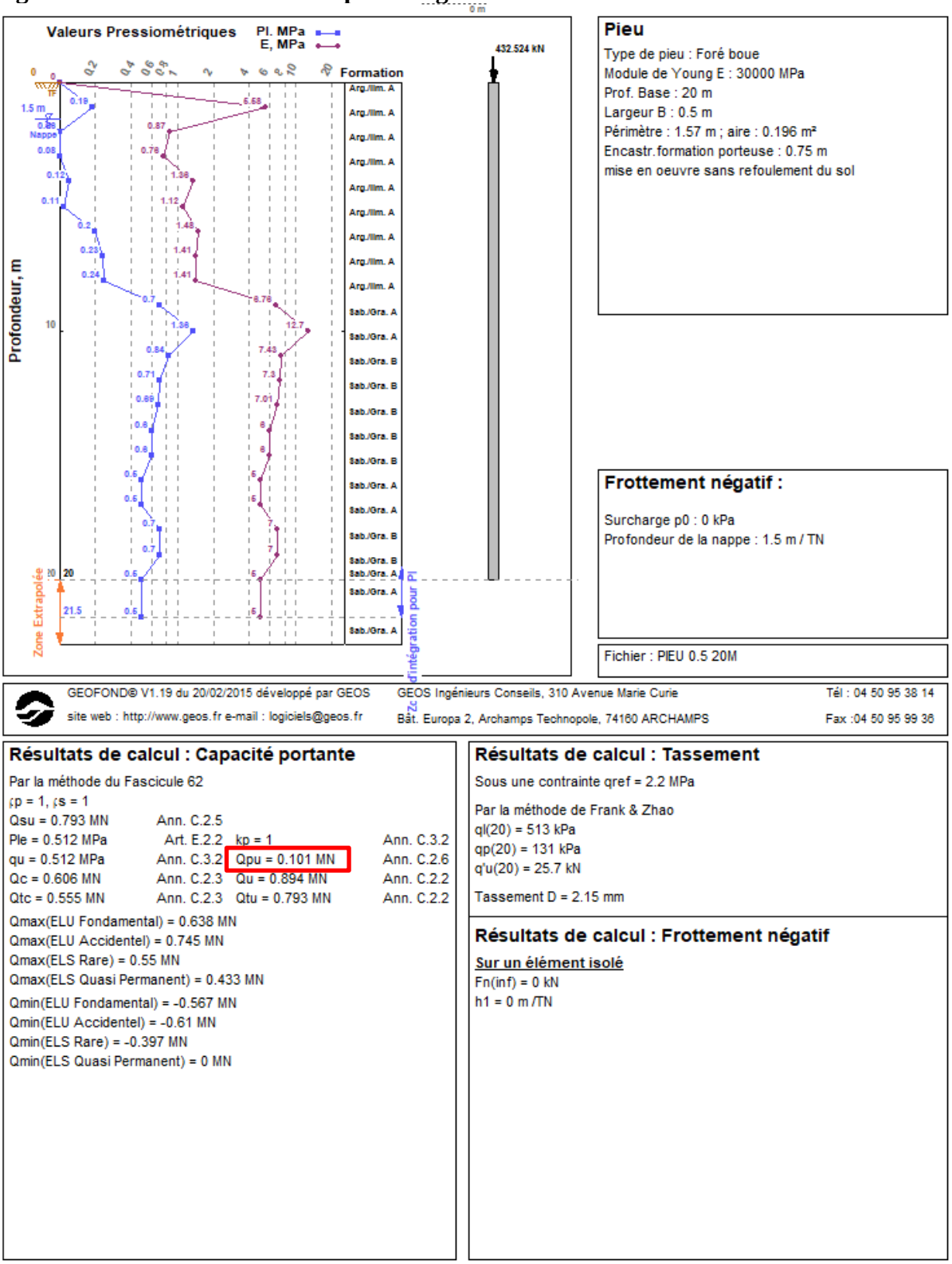

International Journal of Engineering, Sciences and Technologies
ISSN : 3079-2045
https://www.ij-est.org/
Volume 2, issue 3, https://doi.org/10.70961/KNOX5703

**Figure 18. Evaluation of the peak load limit using Excel based on predicted data**

**PIEU FLOTTANT SOUS CHARGE AXIALE (fondation profonde : D/B > 10)**

Fascicule 62 titre V — Résultat prédit par le réseau

**1 RESULTATS ESSAI PRESSIOMETRIQUE (Préssiomètre Ménard)**

| Z (m) | E [Mpa] | Pl [Mpa] |
|---|---|---|
| 1 | | 0,19 |
| 2 | | 0,06 |
| 3 | | 0,08 |
| 4 | | 0,12 |
| 5 | | 0,11 |
| 6 | | 0,20 |
| 7 | | 0,23 |
| 8 | | 0,24 |
| 9 | | 0,70 |
| 10 | | 1,36 |
| 11 | | 0,84 |
| 12 | | 0,71 |
| 13 | | 0,69 |
| 14 | | 0,60 |
| 15 | | 0,60 |
| 16 | | 0,50 |
| 17 | | 0,50 |
| 18 | | 0,70 |
| 19 | | 0,70 |
| 20 | | 0,50 |
| 21 | | 0,51 |
| 22 | | 0,51 |
| 23 | | 1,02 |
| 24 | | 1,04 |
| 25 | | 1,05 |
| 26 | | 1,04 |
| 27 | | 1,04 |

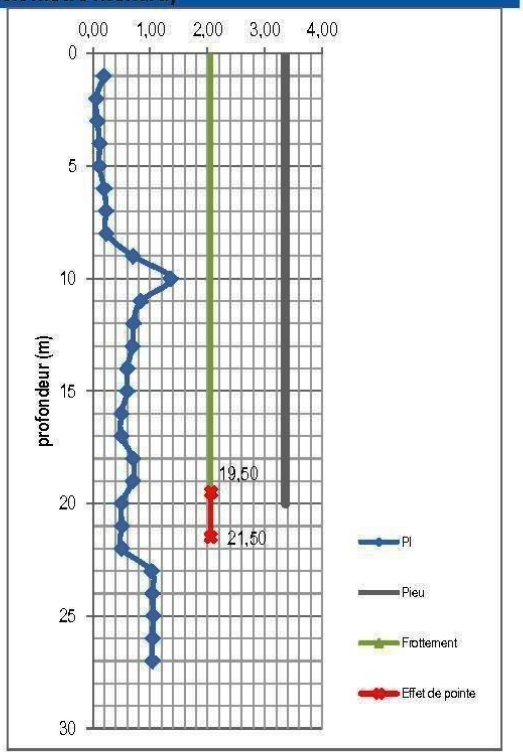


**2 CARACTERISTIQUES DU PIEU**

| | | | | |
|---|---|---|---|---|
| Géométrie du pieu | Circulaire | B = | 0,50 | m |
| | | P = | 1,57 | m |
| | | S = | 0,20 | m² |
| Longueur du pieu dans le sol | | D = | 20 | m |
| Type de mise en œuvre du pieu | | Pieu bétonné sous boue | | |
| Caractéristique du pieu | | Pieu béton | | |
| Si différent de pieu béton (*) | | Sables | | |
| Mise en œuvre du pieu | | Mis en oeuvre sans refoulement du sol | | |
| ancrage du pieu dans la couche porteuse | | h = | 0,75 | m |

**3 CARACTERISTIQUES DU SOL**

| | | | |
|---|---|---|---|
| Type du sol d'assise | Sables - Graves - A | | |
| Facteur de portance du sol | Kp = | 1,00 | |

**4 CHARGE LIMITE DE POINTE : Qp**

| | | | |
|---|---|---|---|
| Paramètres | a = | 0,50 | m |
| | b = | 0,50 | m |
| Bornes d'intégration de la pression limite équivalente | D - b = | 19,50 | m |
| | D + 3a = | 21,50 | m |
| Pression limite nette équivalente | Ple* = | 0,517 | Mpa |
| contrainte de rupture sous la pointe | qu = | 0,517 | Mpa |
| **Charge limite de pointe** | **$Q_{pu}$ =** | **0,1015** | **MN** |

International Journal of Engineering, Sciences and Technologies
ISSN : 3079-2045
https://www.ij-est.org/

Volume 2, issue 3, https://doi.org/10.70961/KNOX5703

**Figure 19. Limit pressure prediction results on the Pr1 diagram**

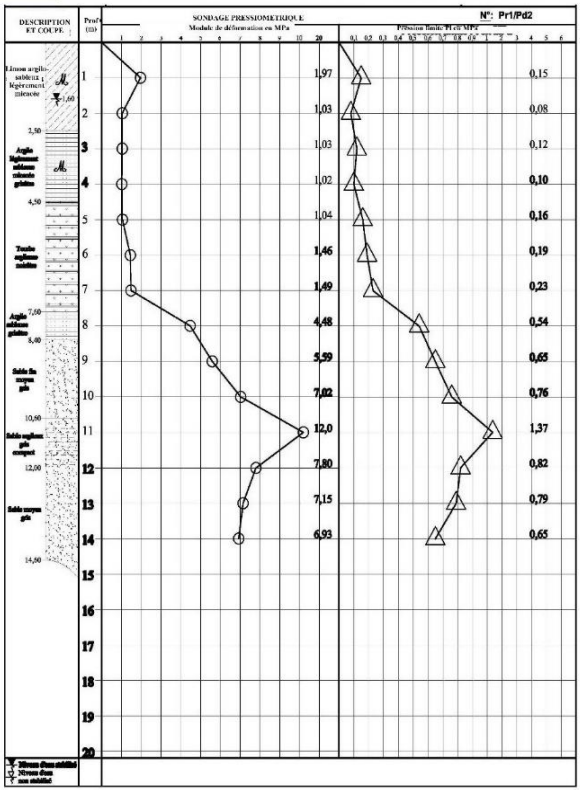


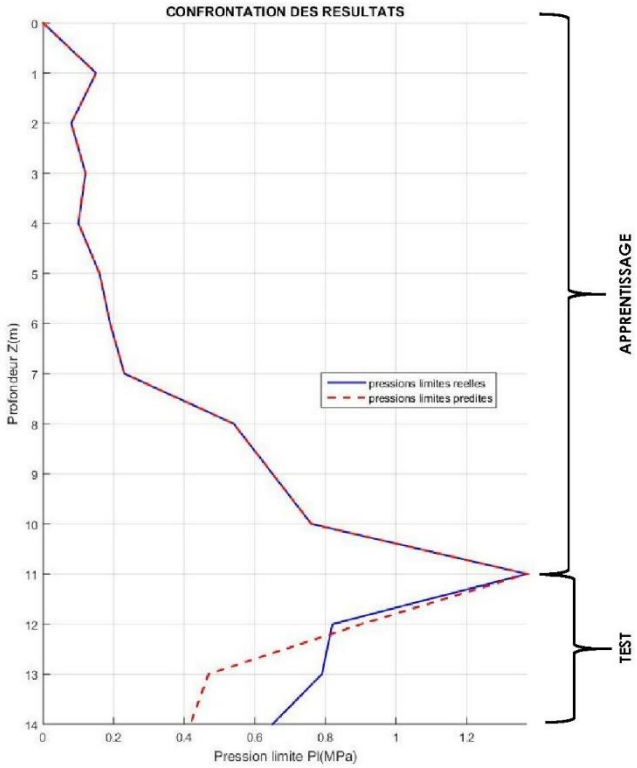


**Figure 20. Limit pressure prediction results on the diagram at PK6+800 between Iavoloha and Ivato**

International Journal of Engineering, Sciences and Technologies
ISSN : 3079-2045
https://www.ij-est.org/
Volume 2, issue 3, https://doi.org/10.70961/KNOX5703

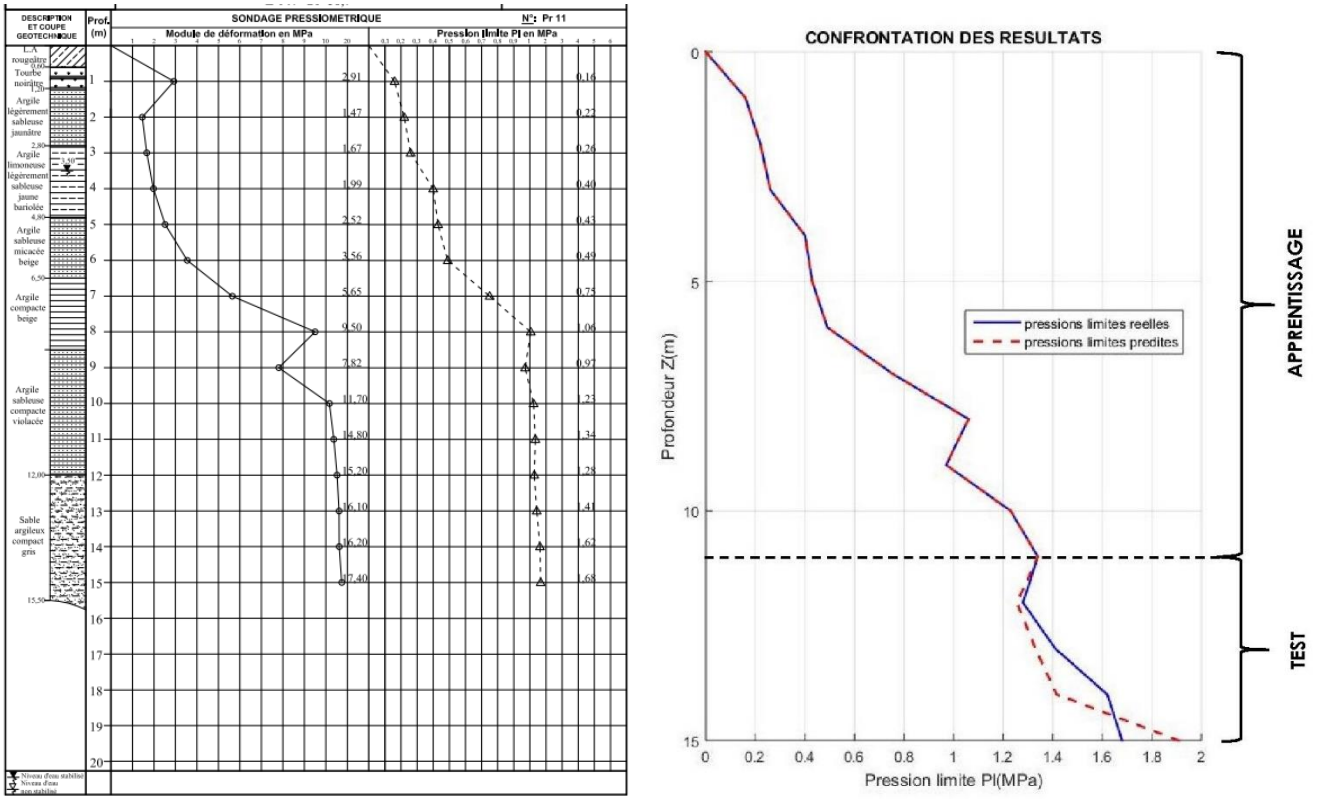


**Figure 21. Results of limit pressure prediction on the diagram of a bridge at Soamanandrariny**